# Wax-Inhibitor Interactions Studied by Isothermal Titration Calorimetry and Effect of Wax Inhibitor on Wax Crystallization

Jost Ruwoldt[1], Sebastien Simon[1], Jens Norrman[1], Hans-Jörg Oschmann[1], Johan Sjöblom[1]

[1]Ugelstad Laboratory, Department of Chemical Engineering, Norwegian University of Science and Technology (NTNU), Sem Sælandsvei 4, N-7491 Trondheim, Norway

**Abstract**

Isothermal titration calorimetry (ITC) is applied to investigate the interactions of polymeric pour-point depressants (PPDs) or asphaltenes with macrocrystalline wax in a model oil system. This represents a novel approach to measure and compare the heat of interaction for solid wax crystals with different wax inhibitors (WIs). In addition, the PPDs were characterized via size-exclusion chromatography (SEC) and differential scanning calorimetry (DSC), and the effect of PPDs or asphaltenes onto the wax appearance temperature (WAT) and the formed wax-oil gel was investigated using DSC, cross-polarized microscopy (CPM), and rheometry. The results show that there is detectable interaction heat with wax crystals for all PPDs, and asphaltenes. DSC and viscometry show a decrease in observed WAT for all WIs as compared to the additive-free blank case. CPM imaging shows differences in structure, shape, and size of the wax crystals formed in presence of particular PPDs or asphaltenes, which is also seen as a decrease in gel-breakage strength. Overall, there is no direct correlation between interaction heat and WI performance characteristics, such as a high decrease in WAT or gel strength. Ethylene-vinyl acetate copolymer (EVA) with 25 % vinyl actetate accounts for the highest interaction heat measured, but shows effective decrease in wax crystals size for only part of the crystals while acting as a flocculate to others, which resulted in a low effect on gel strength. Commercial PPDs based on polycarboxylate have the best performance for the model oil system used, but show only overage interaction heat values. The interaction heat of asphaltenes with wax is measurable, but lower than for the PPDs tested. The presence of asphaltenes significantly lowered the gel strength and changed the wax crystal morphology to rounder and dendrite like shapes. These findings suggest that asphaltene compounds are incorporated into the wax crystals, changing the structure and shape of the crystals.

## 1. Introduction

In the production of waxy crude oil, paraffin wax poses challenges when the oil is cooled below wax appearance temperature (WAT), due to the formation of solid wax crystals. Problems related to wax in crude oils include the formation of a wax deposition layer, and gel formation during pipeline shut-in [1]. The worst case is a plugged pipeline, which can cause sever costs for replacement and downtime [2]. Strategies employed to manage and prevent problems associated with waxy crude oils can be grouped

into thermal, chemical and mechanical measures [3]. Thermal measures seek to heat or maintain the oil above WAT, whereas mechanical measures remove the deposit by scraping or cutting the deposit. Pigging is the most prominent form of mechanical wax removal [4]. Research has been done on non-wax-stick coating [5], fused chemical reactions [6], microwave heating, as well as acoustic and ultrasonic treatment [7]. Polymeric type wax inhibitors (WIs) and pour-point depressants (PPDs) are among the most commonly applied chemical measures to prevent gelling and high viscosity fluids that would obstruct crude oil production [8]. The terms WI and PPD are used as synonyms, even though there is a slight difference in etymology and meaning [9]. Generally speaking, WIs are substances that are used to prevent or alleviate problems associated with the crystallization of wax, whereas PPDs are substances that reduce the pour-point of a given waxy solution. The pour-point is defined as the temperature, at which the liquid loses its ability to flow freely and can be determined using ASTM D97, D5849 or D5949 [10-12]. In this study, the term PPD is used for the commercial and non-commercial polymers that were investigated, whereas WI is used in a general context describing substances that can influence wax crystallization in an advantageous manner.

Wax crystallization takes place in three stages, which are nucleation, growth, and agglomeration [8, 13]. Nucleation usually lags behind the thermodynamic equilibrium, as a result of supersaturation, which has been verified by DSC measurements [14]. Different geometrical shapes have been reported for wax particles that crystallize from organic solvents, including plate shapes, needle shapes and malcrystalline masses [15]. The size and shape of wax particles are reported to depend on factors such as molecular weight and melting point of the waxes, solvent-solute ratio, and the composition of the solution [16, 17]. Depending on the size and shape of the formed crystals, wax types are also categorized into macrocrystalline and microcrystalline wax. Macrocystalline wax is mainly composed of low molecular weight *n*-alkanes ($C_{16}$-$C_{40}$), whereas microcrystalline wax holds significant amounts of high molecular weight *iso*-alkanes and *cyclo*-alkanes [8]. Consequently, macrocrystalline wax tends to form relatively large crystals with high aspect ratios, while microcrystalline wax in comparison tends to form smaller crystals. Both wax types generally differ in WAT, gelation temperature and tensile strength of the formed gel, where macrocrystalline is reported to lead to the formation of strong gels and microcrystalline wax to weak gels [18].

The precise mechanisms of action of WIs and PPDs are unknown, but it is generally assumed that PPDs are included in the growing wax crystals by co-crystallisation to modify their size and shape [9]. The resulting crystal morphology is distorted to an extent, where three-dimensional interlocking of the wax crystals is reduced. Also, the incorporated molecules can prevent particle-particle interactions from forming aggregates or volume spanning networks [19]. The use of PPDs therefore leads to lower gelation temperatures and a lower viscosity of the formed wax-oil gel, which in turn facilitates favorable flow properties and pumpability. Ethylene copolymers are reported as commonly used PPDs [8, 20, 21]. These include chemistries such as poly(ethylene-co-vinyl acetate) (EVA), polyethylene

poly(ethylene-propylene), and poly(ethylene-butene). Additionally poly(maleic anhydride amide co-α-olefin) or coated nanoparticles are mentioned as effective WIs and PPDs [8, 22, 23].

Asphaltenes are defined as a substance group originating from petroleum, coal or shale oil, which is soluble in benzene, but insoluble in low molecular weight n-alkanes [24]. Asphaltene molecules are of high molecular weight and contain polycondensed aromatic rings with aliphatic chains attached [25]. Heteroatoms, such as oxygen, nitrogen, sulfur or certain metals, are found in asphaltenes as well. The effect of asphaltenes on wax precipitation is discussed contradictorily in literature [16]. It has been reported that the presence of asphaltenes decreases pour point and strength of the formed wax-oil gel [26-29]. These results are contradicted by authors stating no synergistic interactions between asphaltenes and waxes [30], and reports about asphaltenes acting as crystallization sites, increasing the WAT and pour-point [31, 32]. Also, an influence of asphaltenes on the efficiency of PPDs is suggested [17, 33], and the dispersion degree of asphaltenes is pointed out as influence on wax crystallization [34].

Isothermal titration calorimetry (ITC) is a technique predominantly used for the study of proteins, ligand binding to proteins and RNA folding [35], to determine e.g. the number of binding sites, equilibrium constants, Gibbs free energy of binding processes, enthalpy or entropy of binding [36]. The method has recently also been applied to petroleum based systems. Wei et al. studied the self-association of asphaltene model compounds [37], the aggregation of tetrameric acid, as well as the interactions of tetrameric acid or different inhibitors with asphaltenes [38-40]. Moreover, Subramian studied the de-aggregation heat of different asphaltene fractions obtained via stepwise precipitation with *n*-hexane or by adsorption and desorption on calcium carbonate [41]. These experiments allowed the study of component characteristics and properties, the quantification of interaction strength between asphaltenes and inhibitor, and the identification of similarities and differences of certain asphaltene fractions.

The goal of this study is to investigate the effect of different WIs and PPDs on wax crystallization and the mechanisms involved, where ITC is used as a novel technique to measure the heat of interaction between paraffin wax and PPDs or asphaltenes, respectively. Size-exclusion chromatography (SEC) and differential scanning calorimetry (DSC) are used to study the polymeric PPDs. DSC, cross-polarized microscopy (CPM), and rheometry are applied to examine the influence of PPDs or asphaltenes onto WAT, crystal morphology, and strength of the formed wax-oil gel. The results allow the comparison of three essentially different measures: (i) Heat of interaction between solid wax and WI, (ii) influence of WI on delayed wax crystallization, and (iii) effect of WI on changing the structure and strength of the resulting wax crystal network.

## 2. Experimental

### *2.1. Materials*

HPLC grade toluene (≥ 99.9 %), n-hexane (≥ 99.7 %), and tetrahydrofuan (THF, ≥ 99.7 %) were obtained from VWR and used without further purification. PPD 1, 2 and 3 are commercial samples

containing petroleum distillate and PPD 5 is a non-commercial PPD, all provided by BASF. PPD 4 was purchased as from Sigmaaldrich. PPD alias and underlying chemistries are listed in Table 1. All PPDs were used without any further treatment. Macrocrystalline wax was obtained as 5405 Sasolwax from Sasol Wax Germany.

*2.2. Sample Preparation*

PPD, asphaltene, and wax solutions were prepared by first weighing the solids and then adding the required amount of solvent. All mass-percentages were prepared to a deviation of ≤ 0.1 wt.%. Prior to use in experiments, complete dissolution of all solids was ensured by heating to at least 20 °C above WAT for at least 30 min. Overall, PPD dosages were designed in excess to ensure a response of the system.

Asphaltenes were precipitated from a crude oil that originated from the Norwegian continental shelf. Prior to preparation, the crude oil was heated to 60 °C for at least 1 h and shaken thoroughly to ensure homogeneity of the sample. 160 ml n-hexane were added to 4 g of crude oil and stirred for a duration of 24 h. The resulting mixture was filtered through a 0.45 µm HVLP-type Millipore filter membrane and subsequently rinsed with hexane until the filtrate was entirely clear. The filter cake was dried for at least 24 h under nitrogen atmosphere. The final yield of asphaltenes accounted for approximately 2.1 wt.% of the original crude oil.

*2.3. Size Exclusion Chromatography (SEC)*

The molecular weight distribution was determined via HPLC with a Shodex KF-803 packed bed column and a Shimadzu SPD-20A UV-detector measuring at a wavelengths of 220 nm and 254 nm. THF was used as bulk solvent at a flow rate of 1 ml/min and calibration was performed using toluene and six Shodex SM-105 polystyrene (PS) standards ranging from 1.22 to 124 kDa, which allowed calculating the relationship between retention time and molecular weight. Injections of 90 µl were done with a sample concentration of 2 g/l and a calibration standard concentration of 1 g/l.

*2.4. Differential Scanning Calorimetry (DSC)*

DSC experiments were conducted on a Q2000 from TA Instruments. The instrument was calibrated by measuring the melting of indium and deionized water. During experiments, the temperature program consisted of heating the sample to 90 °C and keeping at this temperature for 2 min to ensure complete dissolution of the solids, before cooling at a constant temperature gradient. The sealed sample pans were weighed before and after each experiment to check that no sample loss had occurred. Sample concentrations of 5 wt.% macrocrystalline wax and 1000 ppm PPD or asphaltenes in toluene were used.

To determine the WAT, an algorithm was developed in analogy to Kok et al., who defined the detection of a thermal effect under consideration of the thermal noise [42]. In this algorithm, the WAT is defined as the highest temperature, at which three consecutive data points are outside the 99.9 %

confidence interval. In doing so, the assumptions of a linear temperature-heat relationship above WAT, and normal distribution of the thermal noise were made. The confidence interval is calculated as 3.291 times the standard deviation of the heat signal, where the temperature-heat curve is approximated by least squares approximation. The temperature interval is set to 15 °C and moved from higher to lower temperatures for each data point incrementally, while checking for WAT at the lowest temperature of the interval. A schematic of the algorithm is shown in Fig. 1.

### *2.5. Rheological Experiments*

Rheological experiments were performed on an Anton Paar Physica 301 equipped with a 4 cm in diameter 2° cone and plate geometry, which had been sandblasted to provide additional roughness and to prevent slippage. A gap size of 0.170 mm was used in each case. In the method development, previously applied experiment procedures were adapted to the model oil system used in this study [43, 44]. For both experiment types, fast temperature programs were used in order to minimize evaporation of the toluene and assure reproducibility. In comparison to DSC and CPM, the concentrations of wax, PPD and asphaltenes were doubled, to improve the instrument response.

#### *2.5.1. Gel-breakage strength*

The sample was loaded into the rheometer, which was preheated to 30 °C. Cooling took place at a rate of 20 °C/min to 20 °C and subsequently at 1 °C/min to 4 °C. The temperature was held at 4 °C for 2 min before shearing occurred at a rate of 0.1 $s^{-1}$. The gel-breakage strength was defined as the maximum shear stress recorded. Experiments with a ratio of standard deviation to mean value of less than 5 % were conducted twice, all other experiments were conducted at least three times.

#### *2.5.2. Viscometry*

The sample was loaded into the rheometer, which was preheated to 35 °C. A cooling rate of 5 °C/min was applied, while constant shearing at 0.1 $s^{-1}$ occurred. The WAT was determined from the temperature-viscosity curve similar as for DSC, but with a temperature interval of 5 °C. Each experiment was conducted at least three times.

### *2.6. Cross-Polarized Microscope (CPM)*

CPM images were taken with a Nikon Eclipse ME600 microscope fitted with a CoolSNAP-Pro camera by Media Cybernetics and cross-polarization filters. Scaling was done using a stage micrometer. Temperature control of the sample was done with a Linkham PE 94 and LTS-120E peltier system. Concentrations of 5 wt.% macrocrystalline wax and 1000 ppm PPD or asphaltenes in toluene were prepared, filled into capillaries with a cross section of 0.3 x 0.03 mm, and sealed with glue. The temperature program consisted of heating to 60 °C and keeping at 60 °C for 5 min, cooling at 20 °C/min to 30 °C with subsequent cooling at 1 °C/min to 4 °C and keeping at that temperature. Pictures were

taken in the time frame of 30 to 40 min after the sample had reached a temperature of 4 °C. During the temperature cycles, the sample cell was continuously flushed with nitrogen, to avoid the influence of water condensing.

*2.7. Isothermal titration Calorimetry (ITC)*

Isothermal titration was performed on a NANO ITC Standard volume from TA Instruments. The apparatus was calibrated by measuring the heat of reaction for defined titrations of Tris-base with HCl. The reference cell was filled with toluene. All experiments were carried out at a temperature of 20 °C and a stirring rate of 250 rpm. Both sample and reference cell have a volume of 1 ml. Titration took place with a 250 µl syringe in 25 injections, amounting to 10 µl of titrant being added to the sample cell during each injection. The calorimeter was equilibrated to a baseline drift of less than 0.1 µW before each experiment started, which took approximately 30 min for pure solvent in the titration chamber or several hours in case of a wax dispersion. Additionally, 300 s of baseline were recorded before and after each experiment. Data analysis took place in the NanoAnalyze software of TA Instruments. Regions for heat integration were set as the injection instants. For each experiment, the heat generated by frictional losses of the injection was corrected by subtracting reference toluene into toluene injections. All experiments were conducted at least twice to show reproducibility and improve statistical significance.

Solvents and solutions used in ITC were degassed by sonicating for 30 min before use. In addition, PPD, and asphaltene solutions for ITC were prepared one day in advance and stored at room temperature, to ensure complete dissolution and equilibration of the samples. Moreover, these solutions were prepared to 1 wt.% of active content, to ensure comparability and counteract the amount of petroleum distillate contained in the sample. Referencing the amount of active content is a different approach than referencing the total PPD weight as for DSC, CPM, and rheometry. This approach was chosen, because the active content presumably is the interacting fraction in ITC and PPDs were simply added in excess for the other experiment setups. The wax dispersion used in ITC was prepared by heating 10 wt.% macrocrystalline wax in toluene to 100 °C for at least 30 min, and subsequent quenching by immersion in a water bath held at constant 20 °C. After a duration of 1 h, the mixture was removed from the water bath, shaken vigorously for 5 s, and sonicated for 5 s before being filled into the ITC chamber.

## 3. Results and Discussion

*3.1. PPD Characterization*

The molecular weight distributions of PPD 1 to 5 are shown in Fig. 2. The presence of multiple peaks for each sample suggests distinct populations and that PPD 1 to 5 are all polydispersed. PPD 4

and PPD 5 show concurring peaks and similar curve patterns, which is coherent with similarities in their respective chemistries. Analogously, these similarities can also be observed for PPD 1 and PPD 2. For all PPDs there is a considerable amount with a molecular weight below 1000 g/mol equivalent to PS detected, which can be explained as unreacted monomer, polymer with a low degree of polymerization or petroleum distillate contained in the commercial samples. The average molecular weights were calculated by integration using the trapezoid rule and are listed in Table 2. It is to be mentioned, that the molecules greater than 100 000 g/mol equivalent to PS were not separated by the column. Moreover, the assumption is made that molecular weight and absorbance at 220 nm are proportional, and that the confirmation of each sample is the same as for the PS standard. Because of this and due to the presence of monomers, the computed molecular weights in Table 2 are not to be taken as absolute values, but as a measure of comparison within this study.

The DSC profiles show distinct crystallization peaks for the different PPDs (Fig. 3). The according crystallization heat is listed in Table 3 and was determined by integrating from crystallization onset to -50 °C with a linear baseline for each sample. At -50 °C all samples except for PPD 5 showed a qualitative return to the reference profile of pure toluene, so the heat value of PPD 5 has to be considered with caution. The difference in measured heat is approximately within the same range for PPD 1 to 5 when related to active content, but 3 to 6 times lower than for an equivalent wax solution. The crystallization onset was determined using the same algorithm as for the WAT described in section 2.4. The crystallization onset is approximately the same for all PPDs except for PPD 4, which is higher. PPD 1, 2 and 3 show two local maxima, which can either be due to the petroleum distillate contained in the samples or due to polymer fractions of different molecular weight.

Overall, the DSC results are coherent with SEC observations, because multi component mixtures are characterized by a broad crystallization peak in DSC as shown in Fig. 3. Moreover, PPD 1 has a higher crystallization onset temperature than PPD 2, and PPD 4 has a higher onset temperature than PPD 5, which confirms that a higher average molecular weight accounts for a higher onset temperature for polymers of similar chemistries.

### *3.2. Wax Inhibitor Performance*

#### *3.2.1. Wax Appearance Temperature*

The qualitative progression of the DSC heat curve follows a linear decrease with temperature, until the WAT is reached and a broad peak with considerable tailing is measured, as shown in Fig. 4. The addition of PPD 1 and 2 caused both delay and sharpening of the peaks at precipitation onset, as reported in similar studies [45, 46]. The WAT was computed for a variety of cooling rates in DSC and is shown in Fig. 5. The overall trend is that WAT increases with decreasing cooling rates for all samples. PPD 1 to 5, and asphaltenes lower the WAT as compared to the blank sample without WI. The highest decrease is measured for PPD 1, which decreases the WAT by about 6 °C for all cooling rates. Asphaltenes show

the lowest decrease for cooling rates of 10 °C/min and lower, and PPD 4 has the second lowest decrease for cooling rates in between 8 °C/min and 3 °C/min. Determining an overall ranking is difficult, as for example PPD 5 shows the lowest decrease in WAT at 20 °C/min, but the second largest decrease at 1 °C/min as compared to the WI-free blank sample. The fact that the WAT-cooling rate curves have different slopes and shapes implies that there are differences in the kinetics involved for causing the nucleation lag.

The standard deviation for the DSC results is the greatest at the lowest and highest cooling rates, respectively. High cooling rates, such as 20 °C/min, have a considerably lower resolution, due to a fixed data sampling rate at 0.1 $s^{-1}$, which leads to less accurate determinations of the WAT. In contrast to that, low cooling rates have a high resolution, but a lower signal to noise ratio, since the heat signal is approximately proportional to the cooling rate. The result of this can be seen by the increase in standard deviation at lower cooling rates.

The WAT measurements via viscometry are displayed in Fig. 6 and have a similar trend as comparable DSC results at the same cooling rate. In both cases, PPD 1 accounts for the highest and asphaltenes for the lowest decrease in WAT. All PPDs and asphaltenes show a lower WAT than the WI-free blank sample. PPD 2, 3, 4 and 5 are within the standard deviation similar in value. The model oil contained twice the amount of wax as compared to DSC measurements, in order to increase the sensitivity of the measurement. To ensure comparability, the ratio of PPD or asphaltenes to wax was kept constant.

Both DSC and viscometry show a decrease in WAT for the addition of PPD 1 to 5 or asphaltenes. Such a decrease can be attributed to the change in solubility equilibrium as a result of the formation of solute complexes [47]. This will lead to favorable conditions during crude oil production, where wax deposition may not be a problem as the crude oil temperature does not drop below the WAT. Still, so called thermodynamic wax inhibitors (TWI) are required in high volumes, which can cause these to be uneconomical [48]. The use of crystal modifying WIs is therefore favorable to TWIs, because these are used in concentrations as low as parts per million. In conclusion, investigating the effect of WI on WAT contains valuable information, but the effect on the strength of the formed gel has to be taking into account as well to fully assess the WI performance.

### *3.2.2. Cross-Polarized Microscopy (CPM)*

Wax crystals are made visible in CPM images as white spots, whereas the dark background can be attributed to bulk solvent or crystal geometries and orientations, where the polarized light is not sufficiently depolarized. In Fig. 7 the influence of different PPDs or asphaltenes onto the wax crystal morphology is shown and compared to the blank case with no WI. Wax crystals formed without additives show plate and needle like structures similar to CPM images reported in other studies [49-51]. The intensity and amount of white spots in an image can also provide ground for the estimation of the

amount of wax precipitated [49]. Addition of PPD 1 and PPD 2 therefore suggests the lowest amount of wax precipitated, which shows as crystals of a few micrometer or less in diameter, which are smaller than for the other samples tested. PPD 3 and asphaltenes show a morphological change to more compact, round and dendrite shaped crystals as compared to the plate or needle shapes observed for the case with no WI. PPD 5 shows no qualitative change in morphology. As good functioning pour-point depressants are changing the morphology to preferably smaller crystals with lower propensity to overlap, a ranking can be made based on the CPM images in which PPD 1 and 2 are the best working WIs, and PPD 3 and asphaltenes are working WIs with a lower performance than the first two. Investigating the effect of PPD 4 onto wax crystallization, two groups of crystals with distinct morphologies were found. The first group is composed of structures that are smaller and more compact than crystals formed without WI. The second group displays shapes with a stearic center and several branches, which can be described as plates or flakes joined together. These crystals are greater in size than crystals observed in case of no added WI. Similar crystal aggregates are reported for PPD treated crude oils [17, 50] and are also observed for crystals formed in presence of asphaltenes, but smaller in size. PPD 4 therefore seems to achieve the desired effect for part of the crystals, and act as a flocculent to others. This can for example be explained by premature consumption of the polymer through co-crystallization, since PPD 4 displayed the highest temperature for the crystallization onset as shown in the DSC profile of Fig. 3. Another explanation would be to assume that the polymer is able to act as a steric hindrance as well as a steric connector to wax crystals.

#### *3.2.3. Gel-Breakage Strength*

The results of the gel-strength measurements in Fig. 8 show the influence of the different PPDs, and asphaltenes on the strength of the wax-crystal structure formed. The shape of the stress-strain curve showed an initial linear response, followed by a maximum with subsequent decrease in shear stress as shearing continues, which is in agreement with reports on similar investigations [44, 45, 52]. The best performance is attributed with PPD 1 and 2, as the waxy model oil remained free-flowing even at 4 °C. The lowest gel-strength was measured for asphaltenes, but also PPD 3 lowered the gel-strength to less than one third of the WI-free case. These results are in agreement with the results from CPM imaging. Adding PPD 4 to change the crystal morphology to many small and a few big crystals yielded a decrease to around 75% of the gel strength without additives. The flocculated crystals therefore seem to interlock, forming a gel of considerable strength. No qualitative change in crystal morphology for PPD 5 is confirmed by the least influence on lowering the gel-strength from the WI-free blank case.

### 3.3. *Inhibitor-Wax Interactions*

PPD solutions of different concentrations were prepared prior to ITC analysis to determine the solubility limit. At a ratio of 1 wt.% active PPD in toluene, none of the samples showed precipitated solids after a duration of more than 10 days.

### *3.3.1. Wax Inhibitor Dilution and Dissociation*

The ITC results displayed in Fig. 9 show that injections of PPD or asphaltenes into toluene can follow three distinct patterns. The titration heat for injecting asphaltenes in toluene into toluene is similar to the dissociation of asphaltenes aggregates reported in earlier works [39]. After subtracting the heat values of the reference toluene in toluene injection, the heat calculated for each injection of PPD 4 or PPD 5 in toluene into toluene is below detection limit. PPD 1, 2 and 3 all follow a trend in which the dilution is exothermic in the beginning, but becomes endothermic at injection 2 or 3 with absolute heat values decreasing towards later injections. This pattern could be interpreted as an indication that PPD 1, 2 and 3 associate in toluene. When the solution of PPD in toluene is injected into pure toluene, the associates formed are dissociating, giving an endothermic signal. Another explanation would be that the injection of PPD 1, 2 and 3 shows the dilution heat of the petroleum distillate contained in these samples.

### *3.3.2. Injections into Wax Dispersion*

A CPM image of the wax dispersion as used in ITC experiments is shown in Fig. 10. The image shows the typical morphology of macrocrystalline wax with predominantly plate and needle shaped crystals. It is to be noted that this sample was not filled in a capillary like the other samples, but directly injected onto a microscope slide kept at 20 °C.

The injection interval required for wax dispersions is longer than for injections into toluene, as re-dissolution of wax is a kinetically slower process. Too long injection intervals aggravate the influence of solvent evaporation, so the decision is a trade-off. At injection intervals of 30 min, initial injections did not fully equilibrate for PPD 3 and 5, but towards later injections PPD 1 to 5 had equilibrated before the next injection, as can be seen in Fig. 11. Injections of pure toluene, and of asphaltenes in toluene into the wax dispersion were set to an interval span of 60 min, which is shown in Fig. 12. With this setting, the transferred heat did not reach a steady value for all injections, but the overall baseline drift was negligibly small, obtained value were reproducible, and the recovered cell volume was approximately the same as the input.

Injections of PPD 1, PPD 2 or asphaltenes in toluene into the wax dispersion are qualitatively similar to the injection of pure toluene into the wax dispersion. Injections of PPD 3 and 5 show two local minima for injections 2 to 6, of which the first minimum is the direct response to the injection and the second minimum is a delayed exothermic process. During these injections, equilibrium is not reached

at the end of each interval, so a part of the interaction heat is expected to not be attributed correctly. Still the injection intervals were kept at 30 min for better comparability. The injection of PPD 4 is different from the other samples, because the initial endothermic response right after injection is followed by an exothermic peak for every injection. Similar as for PPD 3 and 5, this indicates two phenomena happening at different kinetic rates. The heat signals for PPD 1 and PPD 2 show only one local minimum during each injection interval. For PPD 1 to 5 the heat signal equilibrates within a fraction of the injection interval towards the end of the experiment, which is different for the injection of pure toluene into the wax dispersion. This indicates, that either the heat released from inhibitor-wax interactions is cancelling out with the heat required for re-dissolution, or that the polymer is inhibiting solid wax from re-dissolving.

*3.3.3. Interaction Heat*

The heat of interaction was calculated as net enthalpy in analogy to Wei et al. [38], where the heat of titrating inhibitor into toluene ($\Delta H_{Int}$) and the heat of titrating toluene into wax dispersion ($\Delta H_{Wax}$) is subtracted from the heat measured when titrating inhibitor into the wax dispersion ($\Delta H_{Total}$), as shown in eq. (1).

$$\Delta H_{Int} = \Delta H_{Total} - (\Delta H_{Inhibitor} + \Delta H_{Wax}) \quad (1)$$

The calculated interaction heat for all PPDs or asphaltenes with wax is exothermic. Fig. 13 shows the average values with according standard deviation. The resulting standard deviation is calculated according to the propagation of error. The first injection is generally disregarded, as diffusion into the syringe tip during equilibration skews the result of the first injection. The highest interaction heat was measured for PPD 4 and the lowest heat values are attributed with asphaltenes. PPD 1, 2, and 5 are within the standard deviation similar and PPD 3 is on average lower than these until injection 10. The maximum interaction enthalpy would be expected to occur at injection 2, because of the highest abundance of unreacted reagent in the reaction chamber. Still the highest interaction enthalpy is measured later than at injection 2 for all PPDs, and asphaltenes except for PPD 1. This supports the idea that reaction kinetics are as slow as that initially part of the interactions take place after consecutive injections. All samples are approaching zero net heat in the final injections, but only asphaltenes have zero interaction heat with wax within the margin of error at the end.

A screening experiment was conducted to determine the interaction heat of 1 wt.% PPD 4 in toluene with a 1 wt.% macrocrystalline wax in toluene solution, which contained no precipitated wax as the WAT is below 20 °C. The interaction heat was measured to be 9.6 µJ per injection averaged over all 25 injections. In comparison to that, the average interaction heat for PPD 4 with a 10 wt.% wax dispersion

is approximately 17800 μJ per injection. This indicates that the interaction heat measured for PPD 4 with macrocrystalline wax is predominantly due to the interactions of polymer with solid wax.

### *3.4. Comparison of the Different Methods*

The interaction enthalpy highest in magnitude was determined for each sample in ITC and is listed together with comparative numerical results of DSC and rheological measurements in Table 4. PPD 1 and 2 have the highest influence on lowering gel-strength and WAT, and the greatest effect on changing crystal morphology, but both PPDs show interaction heat values at the average of all six samples. The highest interaction heat is attributed with PPD 4, which ranks among the last three for all other experiments as shown in Table 4. The data therefore suggests that for the model oil system used, there is no correspondence between the heat of interaction measured in ITC and WI performance characteristics, such as lowering the WAT or gel strength. This further implies that it is not the ability of the WI to react with the solid wax crystals, but characteristics such as changing the morphology to smaller and more compact crystals with low tendency to interlock, which make up an effective WI or PPD.

It is to be noted, that asphaltenes were shown to interact with the wax. This and the changes in crystal morphology then suggest, that asphaltenes influence the formation of wax crystals by being attached to or incorporporated into the wax crystals. In addition to that, aggregated or dispersed asphaltenes may be present in the liquid, distorting the wax crystal growth to more branched structures without actively being incorporated into the crystals. This would explain the high efficiency of asphaltenes in lowering gel-breakage strength, in contrast to a lower interaction heat compared to PPD 1 to 5.

## 4. Summary and Conclusion

In this work, five commercial and non-commercial PPDs, and asphaltenes were investigated in their interactions with solid wax, and their effect on wax crystallization in a model oil system made up of macrocrystalline wax in toluene. PPD characterization was done using SEC and DSC. The influence of PPD or asphaltenes onto WAT, wax-crystal morphology, and strength of the formed wax-oil gel was measured via DSC, CPM, and rheometry. The interaction heat of PPD or asphaltenes with solid wax was measured by ITC.

The polymeric PPDs were found to have a polydispersed molecular weight distribution. The ITC measurements showed detectable interaction heat with macrocrystalline wax for all samples. The highest interaction heat was measured for PPD 4, which is EVA copolymer with 25% vinyl-acetate, and the lowest interaction heat was found for asphaltenes. DSC and viscometry showed the ability of all PPDs, and asphaltenes to lower the WAT. PPD 1, which is a polycarboxylate based polymer,

accounted for the highest decrease in WAT, and asphaltenes showed the lowest effect. The influence of additives on lowering the gel-breakage strength was coherent with CPM imaging. PPD 1 and 2 showed the greatest decrease in wax crystal size, which lead to the formation of a suspension with no detectable gel strength at 4 °C. Asphaltenes accounted for a change in crystal morphology to rounder and dendrite like shapes, which lead to the gel strength being decreased to less than 20 % of the gel strength without additives. This and the fact that there was measurable interaction heat for asphaltenes imply, that asphaltenes are attached to or incorporated into the wax crystals. The EVA based samples, PPD 4 and 5, reduced the gel strength by 25 % or less, which is coherent with CPM imaging. This suggests, that PPD 4 is not a good working WI for the model oil system used, despite the fact that this polymer showed the highest interaction heat.

In conclusion, no direct correspondence was found between the interaction heat of PPD or asphaltenes with solid wax and the WI performance, measured as the impact on lowering WAT or strength of the formed wax-oil gel. The ability of WI to co-crystallize with wax is a necessity, but other characteristics, such as changing the wax crystal morphology to smaller crystals with less propensity to interlock, are crucial properties as well.

**Acknowledgements**

This work was carried out as a part of SUBPRO, a Research-based Innovation Centre within Subsea Production and Processing. The authors gratefully acknowledge the financial support from SUBPRO, which is financed by the Research Council of Norway, major industry partners and NTNU. The authors would further like to thank BASF for providing PPD samples and Sasol for providing the wax sample.

**Acronyms**

CPM = cross-polarized microscopy

DSC = differential scanning calorimetry

EVA = ethylene-vinyl acetate copolymer

HPLC = high-performance liquid chromatography

ITC = isothermal titration calorimetry

PPD = pour-point depressant

PS = polystyrene

SEC = size exclusion chromatography

THF = tetrahydrofuan

WAT = wax appearance temperature

WI = wax inhibitor

**References**

1. Aiyejina, A., et al., *Wax formation in oil pipelines: A critical review.* International Journal of Multiphase Flow, 2011. **37**(7): p. 671-694.

2. Huang, Z., et al., *A fundamental model of wax deposition in subsea oil pipelines.* AIChE Journal, 2011. **57**(11): p. 2955-2964.
3. Paso, K.G., *Paraffin gelation kinetics*. 2005: University of Michigan.
4. Venkatesan, R., et al., *The strength of paraffin gels formed under static and flow conditions.* Chemical Engineering Science, 2005. **60**(13): p. 3587-3598.
5. Guo, Y., et al., *An excellent non-wax-stick coating prepared by chemical conversion treatment.* Materials Letters, 2012. **72**: p. 125-127.
6. Singh, P. and H.S. Fogler, *Fused Chemical Reactions: The Use of Dispersion To Delay Reaction Time in Tubular Reactors.* Industrial & Engineering Chemistry Research, 1998. **37**(6): p. 2203-2207.
7. Jemmett, M.R., *Rheology and deposition of heterogeneous organic mixtures: An expansion of "cold flow" research*. 2012, The University of Utah.
8. Yang, F., et al., *Polymeric Wax Inhibitors and Pour Point Depressants for Waxy Crude Oils: A Critical Review.* Journal of Dispersion Science and Technology, 2015. **36**(2): p. 213-225.
9. Oschmann, H.-J., *Das Kristallisationsverhalten von Paraffinen in Abhängigkeit von ihrer Zusammensetzung sowie seine Beeinflussung durch Paraffininhibitoren*, in *Fakultät für Bergbau, Hüttenwesen und Maschinenwesen*. 1998, Technisch Universität Clausthal: Papierflieger.
10. *Standard Test Method for Pour Point of Petroleum Products*. 2017, ASTM International.
11. *Standard Test Method for Pour Point of Crude Oils*. 2016, ASTM International.
12. *Standard Test Method for Pour Point of Petroleum Products (Automatic Pressure Pulsing Method)*. 2016, ASTM International.
13. Machado, A.L.d.C. and E.F. Lucas, *Poly(Ethylene-co-Vinyl Acetate) (EVA) Copolymers as Modifiers of Oil Wax Crystallization.* Petroleum Science and Technology, 1999. **17**(9-10): p. 1029-1041.
14. Paso, K., et al., *Paraffin Polydispersity Facilitates Mechanical Gelation.* Industrial & Engineering Chemistry Research, 2005. **44**(18): p. 7242-7254.
15. Clarke, E.W., *Crystal Types of Pure Hydrocarbons in the Paraffin Wax Range.* Industrial & Engineering Chemistry, 1951. **43**(11): p. 2526-2535.
16. Ariza-León, E., D.-R. Molina-Velasco, and A. Chaves-Guerrero, *Review of Studies on Asphaltene - Wax Interaction and the Effect thereof on Crystallization.* CT&F - Ciencia, Tecnología y Futuro, 2014. **5**: p. 39-53.
17. Yi, S. and J. Zhang, *Relationship between Waxy Crude Oil Composition and Change in the Morphology and Structure of Wax Crystals Induced by Pour-Point-Depressant Beneficiation.* Energy & Fuels, 2011. **25**(4): p. 1686-1696.
18. Zhao, Y., *Shut in and Restart of Waxy Crude Oil Pipelines: Gelation, Rheology Model Development, and Application of Polymer/Ionic Liquid Based Additive.* 2013.
19. Al-Yaari, M., *Paraffin Wax Deposition: Mitigation and Removal Techniques*. Society of Petroleum Engineers.
20. Wei, B., *Recent advances on mitigating wax problem using polymeric wax crystal modifier.* Journal of Petroleum Exploration and Production Technology, 2015. **5**(4): p. 391-401.
21. Guo, X., et al., *Effect of Cooling Rate on Crystallization of Model Waxy Oils with Microcrystalline Poly(ethylene butene).* Energy & Fuels, 2006. **20**(1): p. 250-256.
22. Yang, F., et al., *Hydrophilic nanoparticles facilitate wax inhibition.* Energy & Fuels, 2015. **29**(3): p. 1368-1374.
23. Li, L., et al., *Improvement of oil flowability by assembly of comb-type copolymers with paraffin and asphaltene.* AIChE Journal, 2012. **58**(7): p. 2254-2261.
24. Kokal, S.L. and S.G. Sayegh, *Asphaltenes: The Cholesterol Of Petroleum*. Society of Petroleum Engineers.
25. Ghosh, A.K., et al., *Review on aggregation of asphaltene vis-a-vis spectroscopic studies.* Fuel, 2016. **185**: p. 541-554.

26. Alcazar-Vara, L.A., J.A. Garcia-Martinez, and E. Buenrostro-Gonzalez, *Effect of asphaltenes on equilibrium and rheological properties of waxy model systems.* Fuel, 2012. **93**: p. 200-212.
27. Tinsley, J.F., et al., *Waxy Gels with Asphaltenes 1: Characterization of Precipitation, Gelation, Yield Stress, and Morphology.* Energy & Fuels, 2009. **23**(4): p. 2056-2064.
28. Oliveira, G.E., et al., *The Effect of Asphaltenes, Naphthenic Acids, and Polymeric Inhibitors on the Pour Point of Paraffins Solutions.* Journal of Dispersion Science and Technology, 2007. **28**(3): p. 349-356.
29. Venkatesan, R., et al., *The Effect of Asphaltenes on the Gelation of Waxy Oils.* Energy & Fuels, 2003. **17**(6): p. 1630-1640.
30. Yang, X. and P. Kilpatrick, *Asphaltenes and Waxes Do Not Interact Synergistically and Coprecipitate in Solid Organic Deposits.* Energy & Fuels, 2005. **19**(4): p. 1360-1375.
31. García, M.d.C. and L. Carbognani, *Asphaltene−Paraffin Structural Interactions. Effect on Crude Oil Stability.* Energy & Fuels, 2001. **15**(5): p. 1021-1027.
32. García, M.d.C., *Crude Oil Wax Crystallization. The Effect of Heavy n-Paraffins and Flocculated Asphaltenes.* Energy & Fuels, 2000. **14**(5): p. 1043-1048.
33. Tinsley, J.F., et al., *Waxy Gels with Asphaltenes 2: Use of Wax Control Polymers.* Energy & Fuels, 2009. **23**(4): p. 2065-2074.
34. Lei, Y., S. Han, and J. Zhang, *Effect of the dispersion degree of asphaltene on wax deposition in crude oil under static conditions.* Fuel Processing Technology, 2016. **146**: p. 20-28.
35. Feig, A.L., *Applications of isothermal titration calorimetry in RNA biochemistry and biophysics.* Biopolymers, 2007. **87**(5-6): p. 293-301.
36. Saboury, A.A., *A review on the ligand binding studies by isothermal titration calorimetry.* Journal of the Iranian Chemical Society, 2006. **3**(1): p. 1-21.
37. Simon, S., et al., *An ITC and NMR study of interaction and complexation of asphaltene model compounds in apolar solvent I: Self-association pattern.* Colloids and Surfaces A: Physicochemical and Engineering Aspects, 2016. **494**: p. 108-115.
38. Wei, D., et al., *An ITC study of interaction and complexation of asphaltene model compounds in apolar solvent II: Interactions with asphaltene inhibitors.* Colloids and Surfaces A: Physicochemical and Engineering Aspects, 2016. **495**: p. 87-99.
39. Wei, D., et al., *Interactions between asphaltenes and alkylbenzene-derived inhibitors investigated by isothermal titration calorimetry.* Journal of Thermal Analysis and Calorimetry, 2015. **120**(3): p. 1835-1846.
40. Wei, D., et al., *Aggregation of tetrameric acid in xylene and its interaction with asphaltenes by isothermal titration calorimetry.* Journal of Thermal Analysis and Calorimetry, 2015. **122**(1): p. 463-471.
41. Subramanian, S., et al., *Asphaltene fractionation based on adsorption onto calcium carbonate: Part 2. Self-association and aggregation properties.* Colloids and Surfaces A: Physicochemical and Engineering Aspects, 2017. **514**: p. 79-90.
42. Kok, M.V., et al., *Comparison of wax appearance temperatures of crude oils by differential scanning calorimetry, thermomicroscopy and viscometry.* Fuel, 1996. **75**(7): p. 787-790.
43. Yao, B., et al., *Organically modified nano-clay facilitates pour point depressing activity of polyoctadecylacrylate.* Fuel, 2016. **166**: p. 96-105.
44. Zhao, Y., et al., *Gelation and Breakage Behavior of Model Wax–Oil Systems: Rheological Properties and Model Development.* Industrial & Engineering Chemistry Research, 2012. **51**(23): p. 8123-8133.
45. Jung, T., J.-N. Kim, and S.-P. Kang, *Influence of polymeric additives on paraffin wax crystallization in model oils.* Korean Journal of Chemical Engineering, 2016. **33**(6): p. 1813-1822.
46. Zhao, Y., et al., *Utilization of DSC, NIR, and NMR for wax appearance temperature and chemical additive performance characterization.* Journal of Thermal Analysis and Calorimetry, 2015. **120**(2): p. 1427-1433.

47. Claudy, P., et al., *Interactions between n-alkanes and cloud point-cold filter plugging point depressants in a diesel fuel. A thermodynamic study.* Fuel, 1993. **72**(6): p. 821-827.
48. Bai, Y. and Q. Bai, *Subsea engineering handbook*. 2012: Gulf Professional Publishing.
49. Paso, K.G., et al., *PPD architecture development via polymer–crystal interaction assessment.* Journal of Petroleum Science and Engineering, 2014. **115**: p. 38-49.
50. Wu, Y., et al., *Modified Maleic Anhydride Co-polymers as Pour-Point Depressants and Their Effects on Waxy Crude Oil Rheology.* Energy & Fuels, 2012. **26**(2): p. 995-1001.
51. Emanuele, V., et al., *Wax crystallization and aggregation in a model crude oil.* Journal of Physics: Condensed Matter, 2005. **17**(45): p. S3651.
52. Paso, K.G., *Comprehensive treatise on shut-in and restart of waxy oil pipelines.* Journal of Dispersion Science and Technology, 2014. **35**(8): p. 1060-1085.

## Figures and Tables

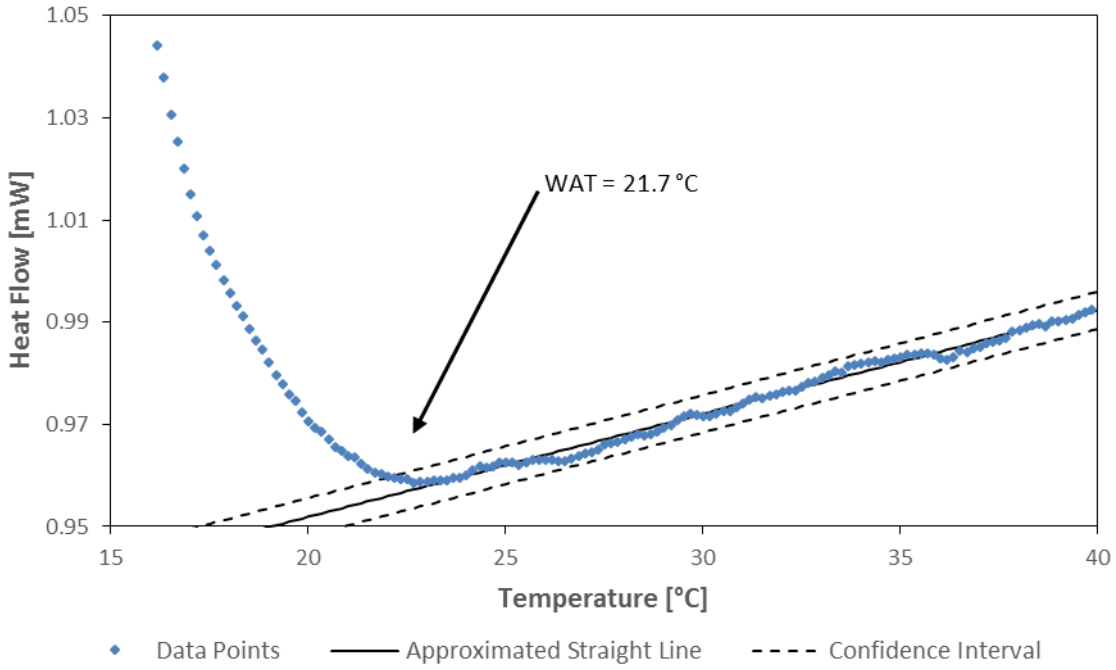


**Fig. 1.** Schematic of WAT algorithm for DSC of 5 wt.% macrocrystalline wax in toluene at a cooling rate of 2 °C/min

**Table 1.** Pour-point depressants

| Alias | Chemistry Based on | Active Content (%) |
|---|---|---|
| PPD 1 | Polycarboxylate | 80 |
| PPD 2 | Polycarboxylate, Maleic Acid | 70 |
| PPD 3 | Polyacrylate, EVA | 50 |
| PPD 4 | EVA, 25 % Vinyl Acetate | 100 |
| PPD 5 | Modified EVA | 100 |

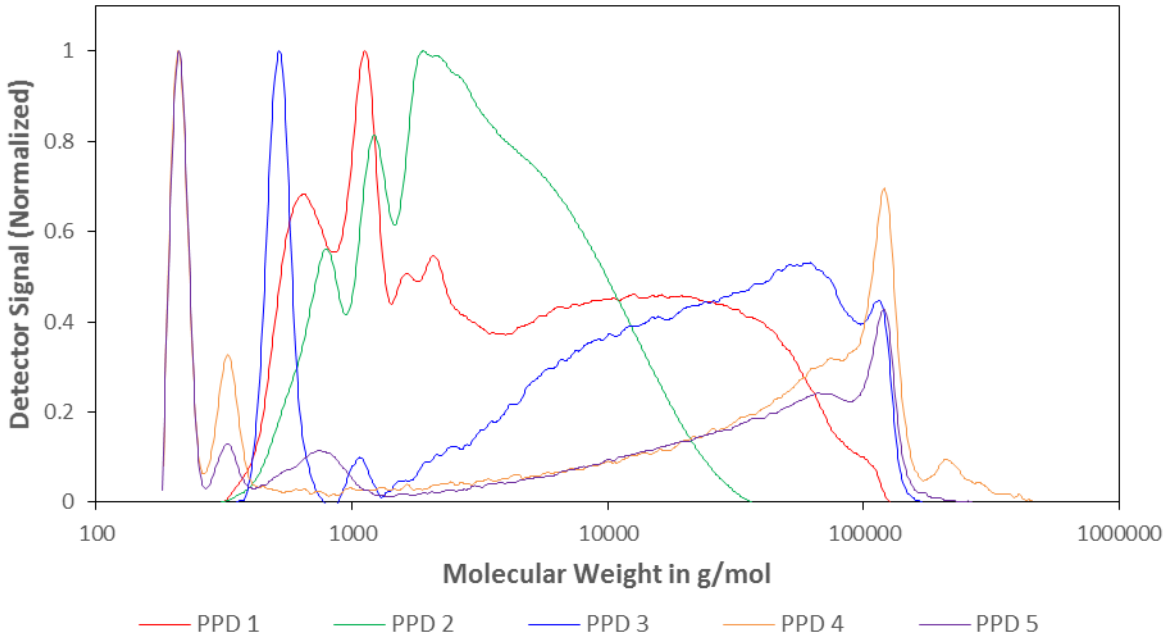


**Fig. 2.** Molecular weight distribution equivalent to PS measured by size exclusion chromatography for all polymer samples; detector signal at 220 nm (normalized to the highest peak)

**Table 2.** Mass and number average equivalent to PS calculated by integration via trapezoidal rule for all polymer samples

| | **PPD 1** | **PPD 2** | **PPD 3** | **PPD 4** | **PPD 5** |
|---|---|---|---|---|---|
| Number Average (kDa) | 41.5 | 9.2 | 67.3 | 117.7 | 90.6 |
| Mass Average (kDa) | 61.9 | 14.1 | 86.8 | 156.9 | 118.4 |

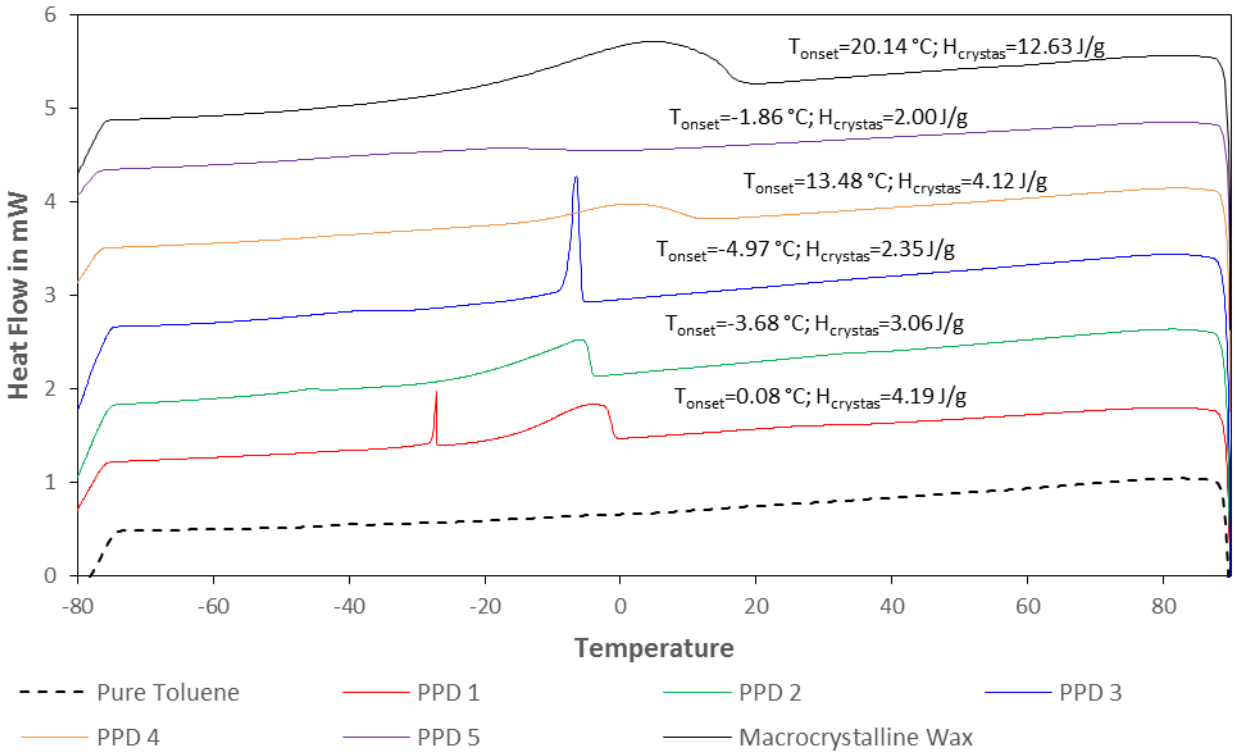


**Fig. 3.** DSC profiles of 5 wt.% substance in toluene at a cooling rate of 5 °C/min

**Table 3.** Crystallization heat and crystallization onset for different PPDs in comparison to macrocrystalline wax measured at a cooling rate of 5 °C/min; all samples use toluene as bulk solvent

| **Substance** | **Crystallization heat (J/g)** | **Crystallization onset (°C)** |
|---|---|---|
| 5 wt.% PPD 1 | 4.2 | 0.1 |
| 5 wt.% PPD 2 | 3.1 | -3.7 |
| 5 wt.% PPD 3 | 2.4 | -5.0 |
| 5 wt.% PPD 4 | 4.1 | 13.5 |
| 5 wt.% PPD 5 | 2.0 | -1.9 |
| 5 wt.% Macrocrystalline Wax | 12.6 | 20.1 |

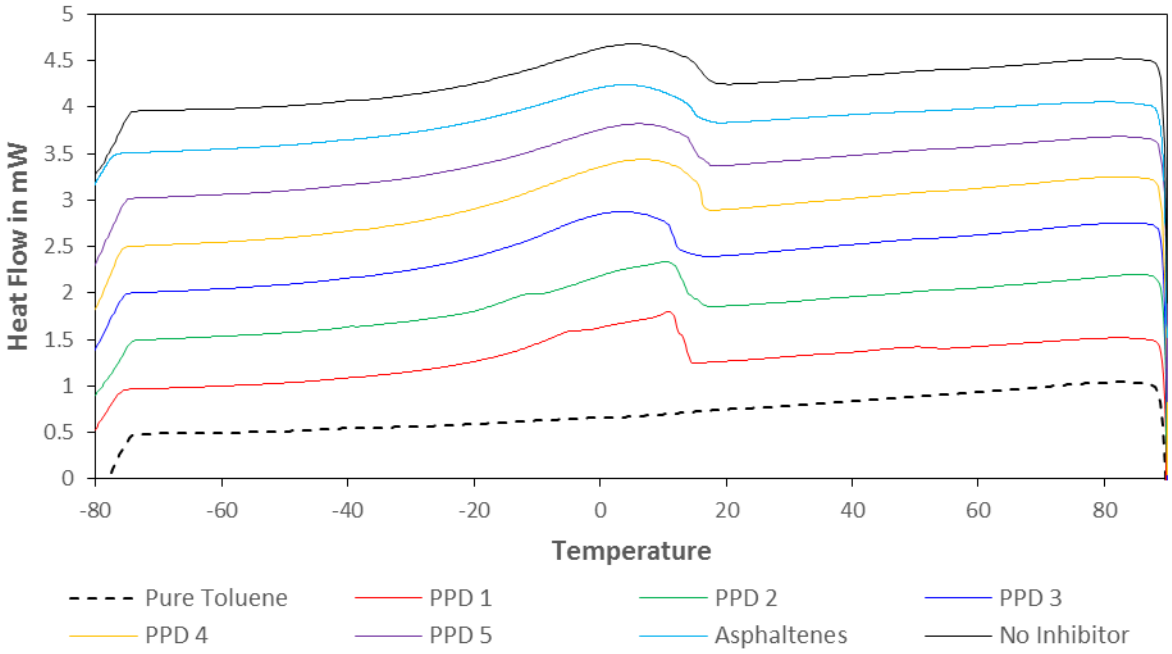


**Fig. 4.** DSC profiles for 5 wt.% macrocrystalline wax and 1000 ppm PPD or asphaltenes in toluene at a cooling rate of 5 °C/min

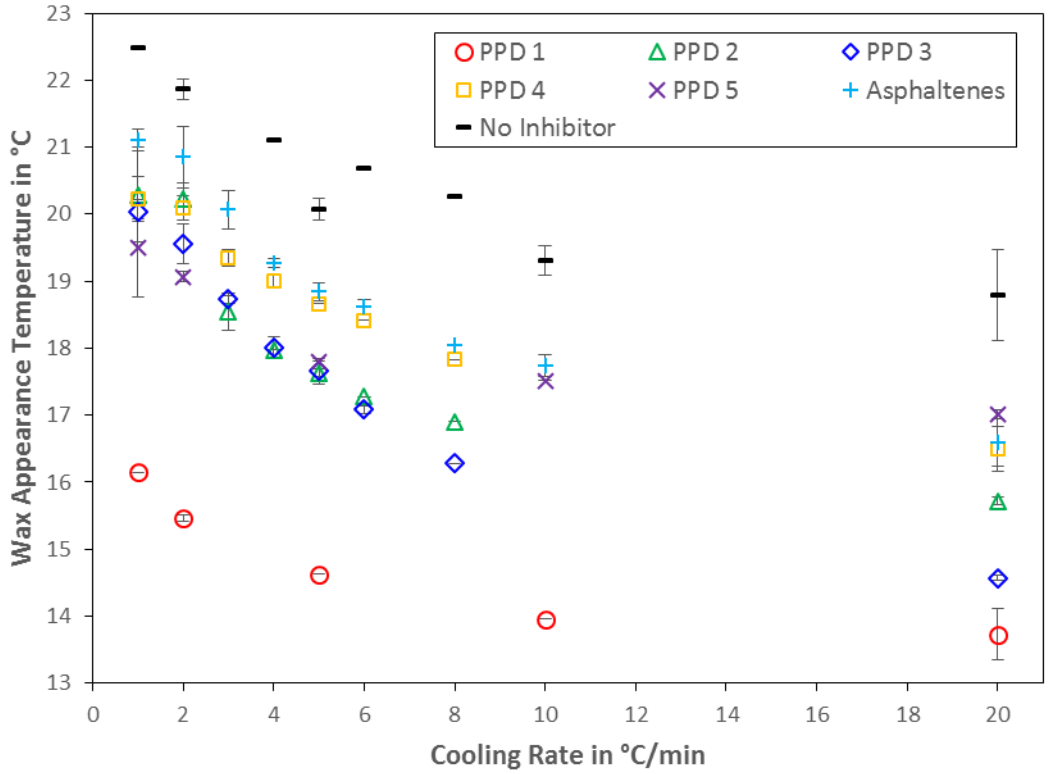


**Fig. 5.** WAT values of 5 wt.% macrocrystalline wax with and without 1000 ppm PPD or asphaltenes measured at different cooling rates using DSC; error bars represent the standard deviation from the average of each measurement

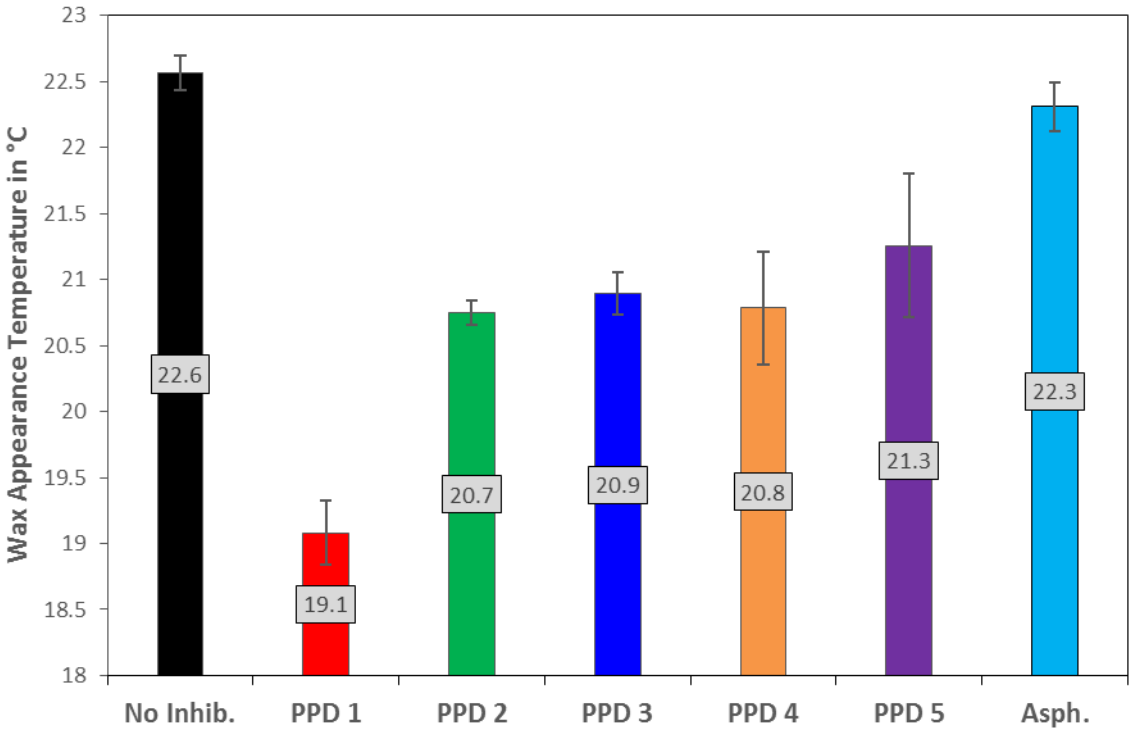


**Fig. 6.** Wax appearance temperatures of 10 wt.% macrocrystalline wax with and without 2000 ppm PPD or asphaltenes measured at a cooling rate of 5 °C/min using viscometry; error bars represent the standard deviation from the average of each measurement

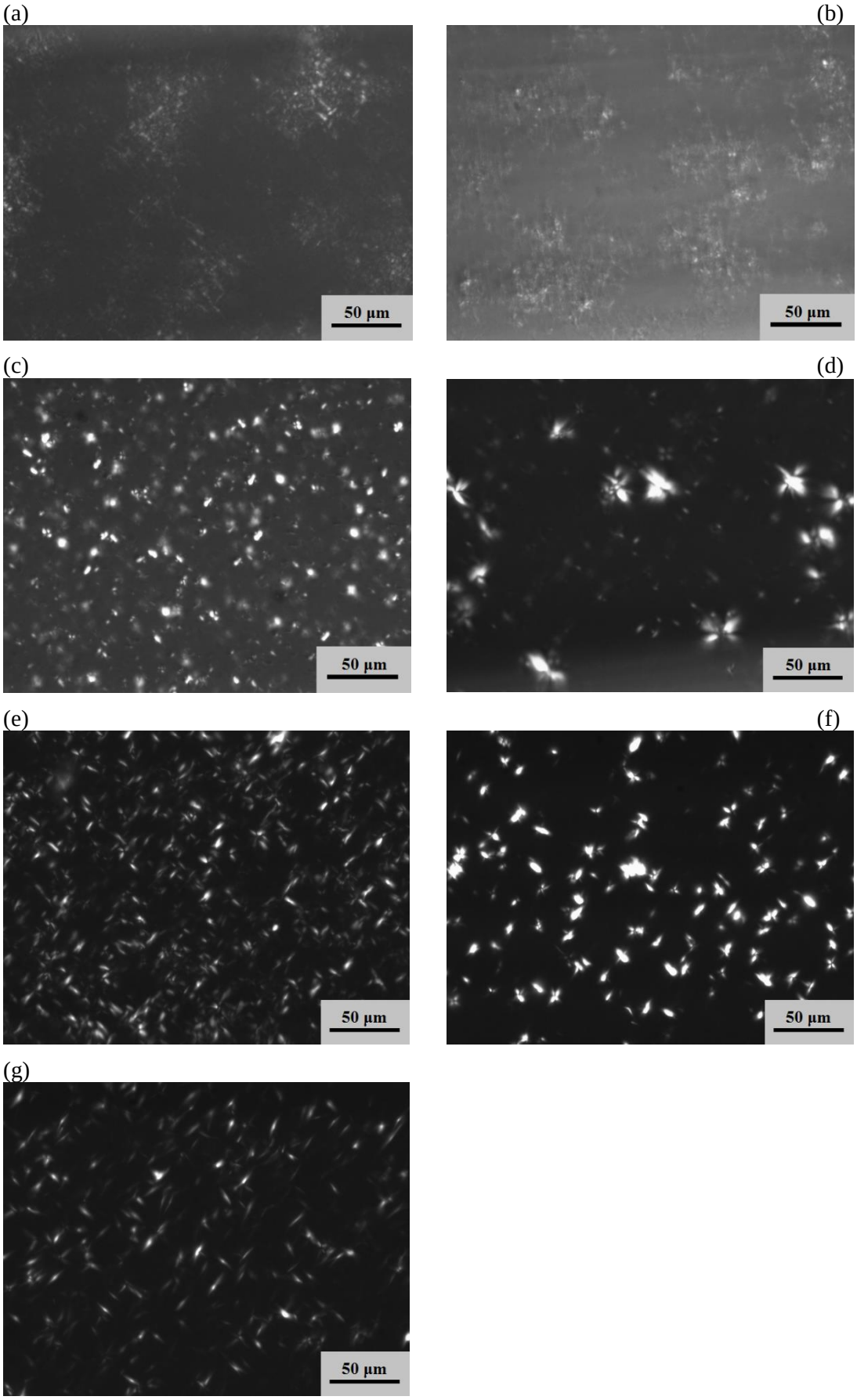


**Fig. 7.** CPM images for 5 wt.% macrocrystalline wax and 1000 ppm PPD or asphaltenes in toluene @ 4 °C, where (a) PPD 1, (b) PPD 2, (c) PPD 3, (d) PPD 4, (e) PPD 5, (f) asphaltenes, and (g) no WI

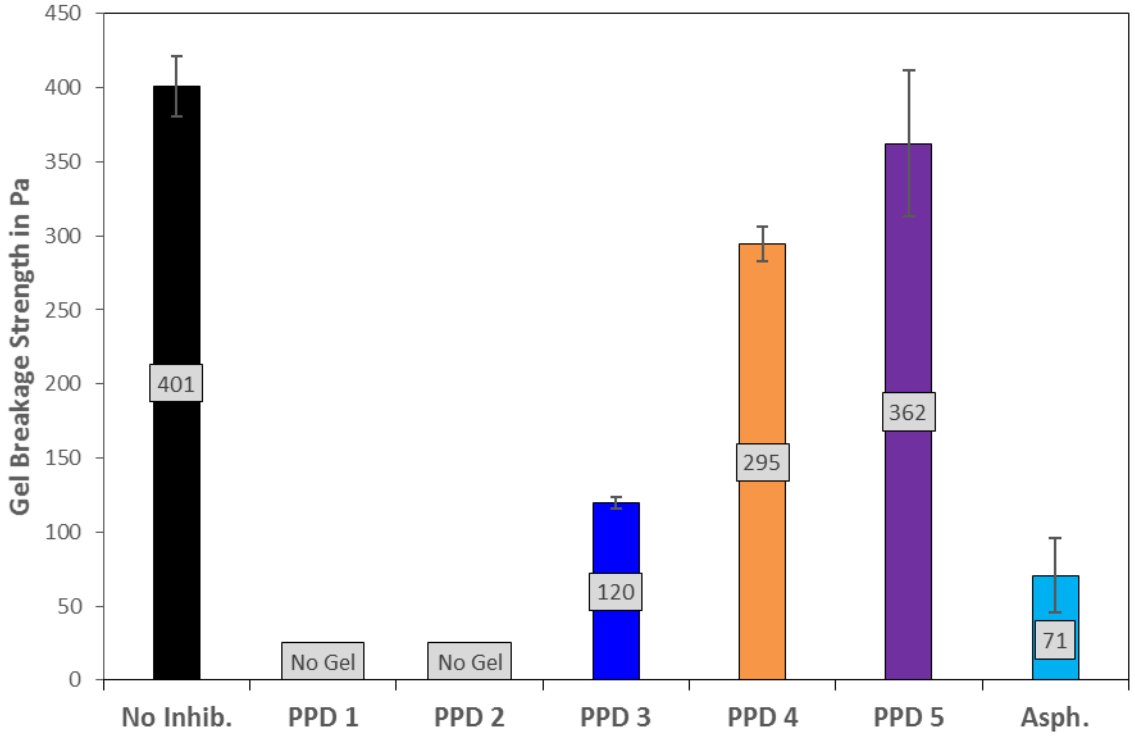


**Fig. 8.** Gel breakage strength of 10 wt.% macrocrystalline wax with and without 2000 ppm PPD or asphaltenes measured at 4 °C; error bars represent the standard deviation from the average of each measurement

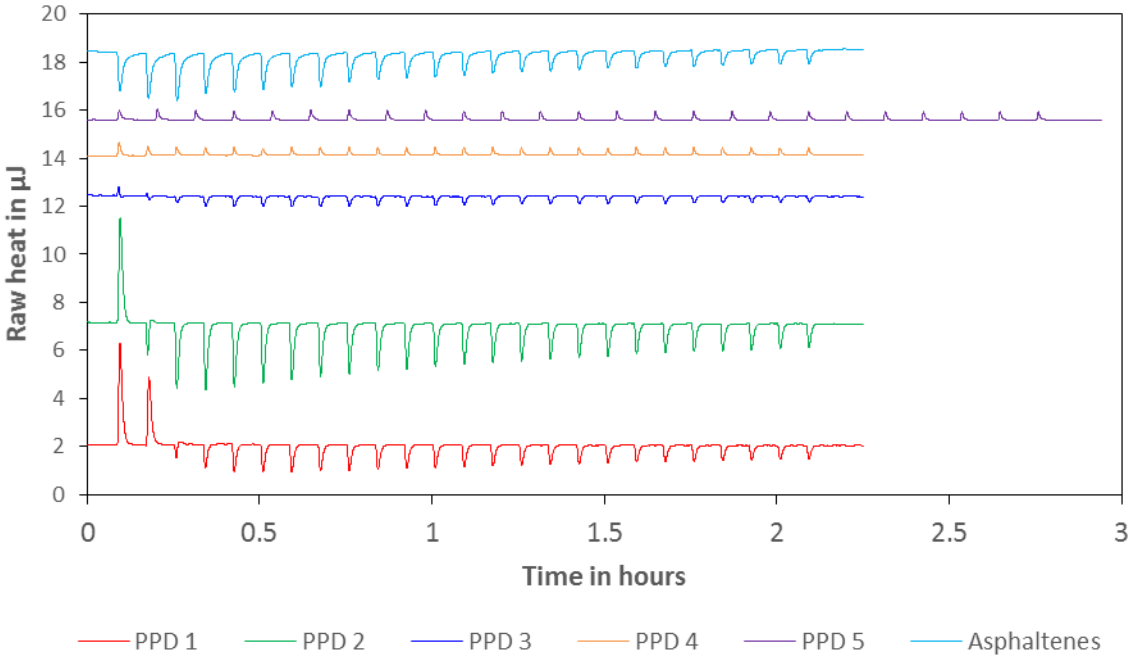


**Fig. 9.** Heat signals for injections of 1 wt.% active PPD or asphaltenes in toluene into pure toluene

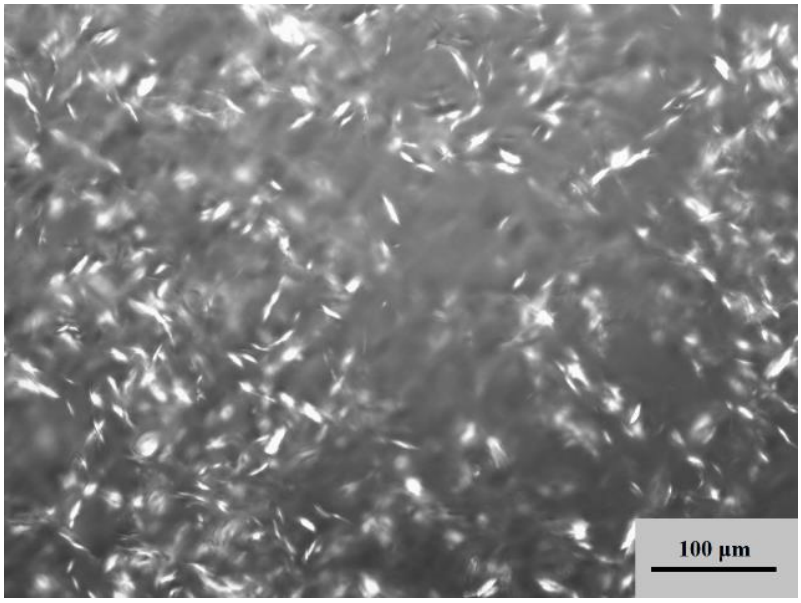


**Fig. 10**: CPM image of 10 wt.% macrocrystalline wax dispersion prepared for ITC experiments at 20 °C

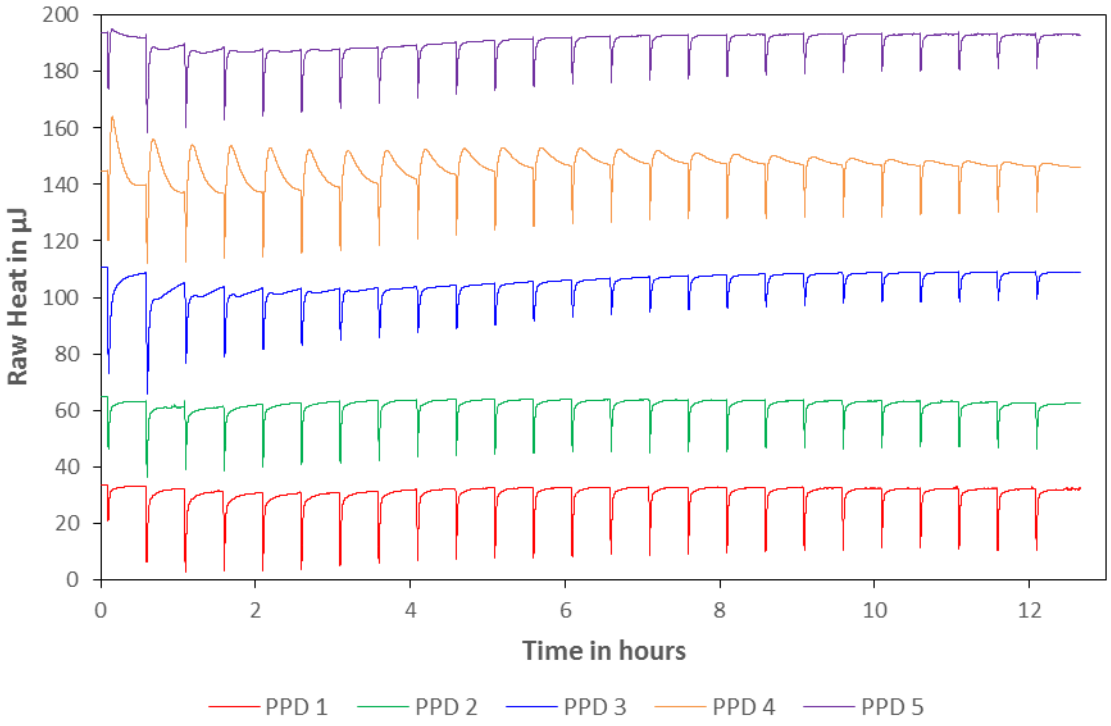


**Fig. 11.** Heat signals for injections of 1 wt.% active PPD in toluene into 10 wt.% macrocrystalline wax dispersion in toluene

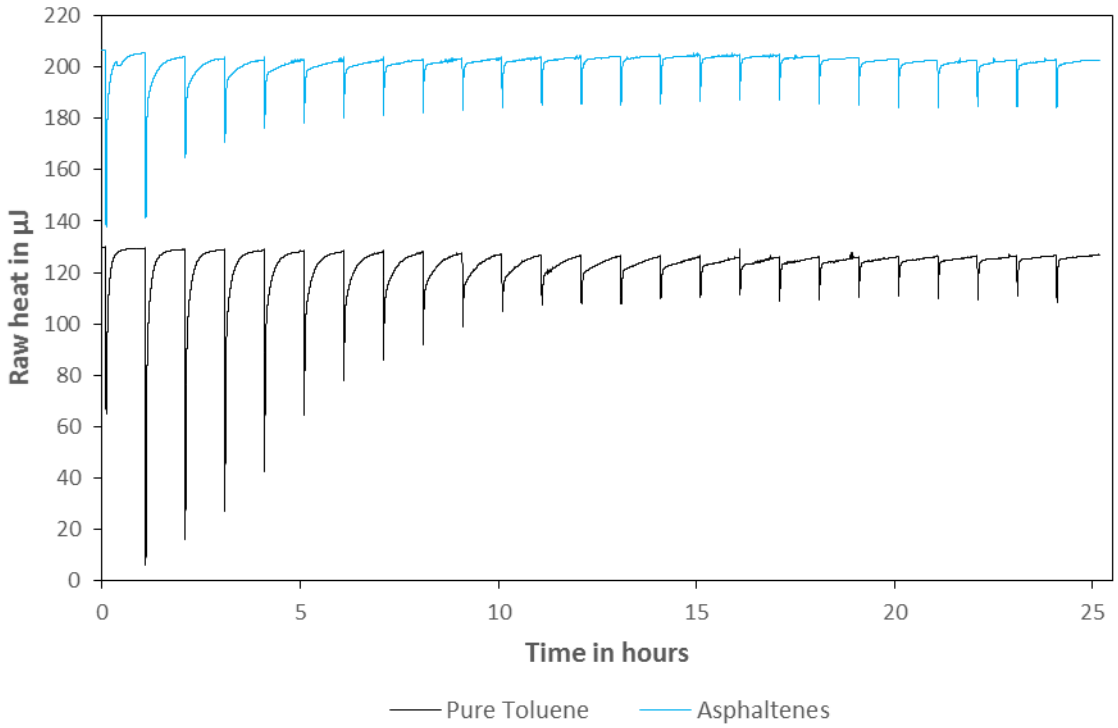


**Fig. 12.** Heat signals for injections of 1 wt.% asphaltenes in toluene or pure toluene into 10 wt.% macrocrystalline wax dispersion in toluene

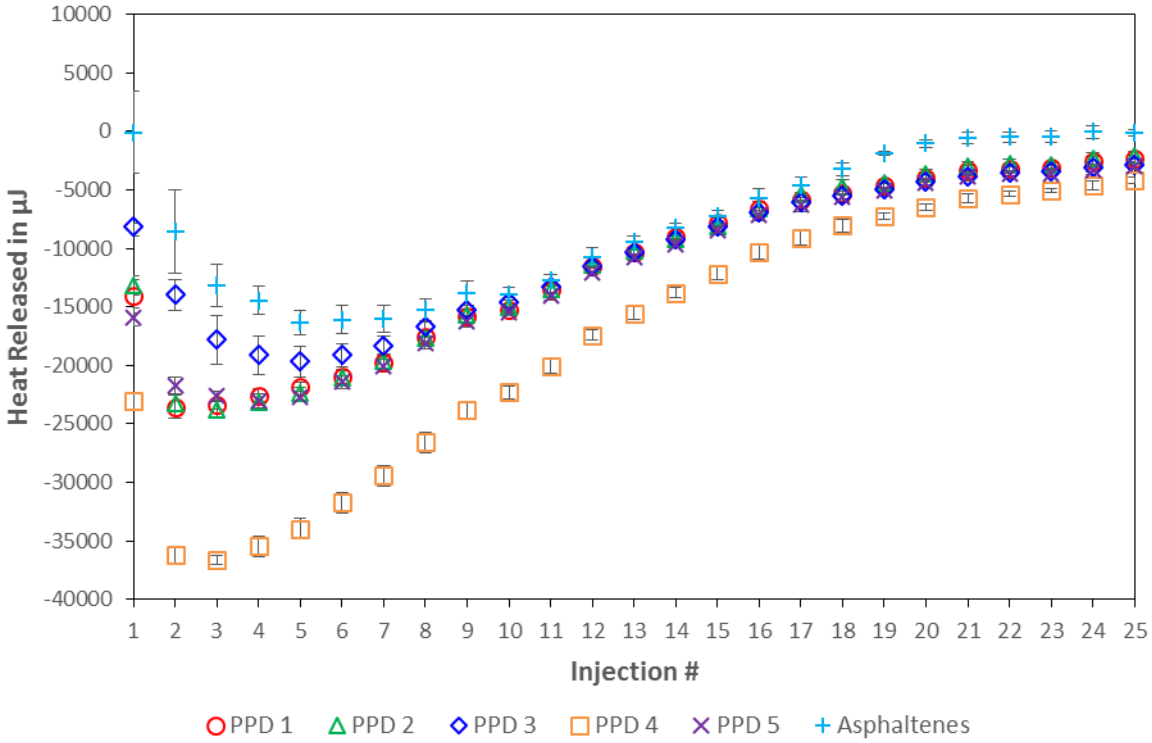


**Fig. 13.** Resulting interaction heat for 1 wt.% active PPD or asphaltenes with 10 wt.% macrocrystalline wax dispersion in toluene; each injection accounts for 10 µl of titrant being added to 1 ml of wax dispersion; error bars represent the standard deviation from the average of each measurement

**Table 4.** Comparison of the final results from ITC, DSC and rheometry

| | No Inhibitor | PPD 1 | PPD 2 | PPD 3 | PPD 4 | PPD 5 | Asphaltenes |
|---|---|---|---|---|---|---|---|
| ITC, maximum interaction heat [mJ] | | -23.6 | -23.8 | -19.7 | -36.6 | -23.0 | -16.4 |
| WAT, DSC, 5 °C/min [°C] | 20.1 | 14.6 | 17.6 | 17.7 | 18.7 | 17.8 | 18.8 |
| WAT, Viscometry, 5 °C/min [°C] | 22.6 | 19.1 | 20.7 | 20.9 | 20.8 | 21.3 | 22.3 |
| Gel-breakage strength [Pa] | 401 | No Gel | No Gel | 120 | 295 | 362 | 71 |
| CPM, crystal morphology | Needle and plate shape | Small, compact | Small, compact | Compact, round | Small and compact or big flakes | Needle and plate shape | Distorted, dendrite like |